Review

Not peer-reviewed version

A Review on Clinical Optoacoustic Imaging: Are We Close to Clinical Adoption?

Sergio Contador , Jorge Ripoll , Eduardo Lage , Juan Aguirre *

Posted Date: 23 April 2024

doi: 10.20944/preprints202404.1202.v2

Keywords: clinical optoacoustic imaging; clinical photoacoustic imaging; clinical translation

 doi:10.20944/preprints202404.1202.v2

Review

A Review on Clinical Optoacoustic Imaging: Are We Close to Clinical Adoption?

Sergio Contador [1,2], Jorge Ripoll [3,4], Eduardo Lage [1,2] and Juan Aguirre [1,2,*]

[1] Departamento de Tecnología Electrónica y de las Comunicaciones, Universidad Autónoma de Madrid, Madrid, Spain
[2] Instituto de Investigación Sanitaria de la Fundación Jiménez Díaz, Madrid, Spain
[3] Departamento de Bioingeniería e Ingeniería Aeroespacial, Universidad Carlos III de Madrid, Leganés, Spain
[4] Instituto de Investigación Sanitaria Gregorio Marañón, Madrid, Spain
* Correspondence: juan.aguirre@uam.es; Tel.: +34914976802

Abstract: Optoacoustic imaging is an emerging technology that holds great promise for improving general clinical practice since it offers a unique combination of optical absorption contrast, high resolution, and high penetration depth. This combination of factors provides a distinct advantage over alternative imaging modalities in oncology, cardiology, dermatology, or endocrinology among other medical fields. Optoacoustic technology affords the medical practitioner the possibility of visualizing light-absorbing biomolecules like water, lipids, oxy/deoxy hemoglobin or melanin in deep tissue with relatively cheap and small form factor instruments, without the need of contrast agents or ionizing radiation. Moreover, exogenous fluorescent contrast agents like indocyanine green or methylene blue can also be observed. Driven by its potential for new applications in the clinic, the field has experienced intense changes in the last 20 years. Continuous technological advancements in instrumentation, image formation methods, or acquisition geometries, have led to the development of numerous clinical devices also motivating the creation of several startup companies that aim to translate the technology from the lab to the clinic. Thus, the question arises: how far are we from clinical adoption? In this article, we aim to shed light on such question by reviewing the clinical studies that have been performed in the last 10 years. Our intention is to go beyond the classical review format by providing a brief general overview of the steps that new imaging methods undergo on their journey from the lab to clinical adoption. Then we examine the progress that optoacoustic technology has made on such a journey.

Keywords: clinical optoacoustic imaging; clinical photoacoustic imaging; clinical translation

1. Introduction

Optoacoustic imaging (OAI) is an emerging optical imaging modality that leverages the combination of the rich contrast based on optical absorption with the ability of ultrasound (US) to provide high resolution images of deep tissue [1–3]. In this technique, tissue is illuminated with low energy optical pulses. As light travels, it is selectively absorbed by chromophores, creating a local increase in pressure via thermo-elastic expansion, which in turn produces US waves. By placing several detectors at the tissue surface, the time profile of the acoustic waves can be recorded. Different image formation methods [4–6] can be used to convert the acoustic signals into 2D or 3D images of regions displaying high optical absorption, even in deep tissues. The combination of the contrast provided by light absorption and US detection allows producing images of medically relevant light-absorbing biomolecules or compounds like melanin, water, and oxy/deoxy hemoglobin, amongst others. Importantly, the depth-to-resolution ratios are the ones typical from US imaging systems (tens of micrometers resolution at few millimeters depth, and hundreds of micrometers at several centimeters depth). Hence, OAI is a molecular imaging technique that uses non-ionizing radiation

 doi:10.20944/preprints202404.1202.v2

and has a "label-free nature" that can be used for frequent monitoring of patients and longitudinal studies. It is important to remark that methylene blue and indocyanine green (ICG), which are long-standing FDA-approved optical contrast agents with different clinical prescriptions, exhibit a strong optoacoustic effect and thus, can be imaged by OAI systems.

Despite the wealth of modern imaging alternatives, other modalities simply cannot obtain the distribution of relevant biomolecules under the same conditions of contrast, specificity, safety, resolution, and depth. Positron emission tomography or single-photon emission computed tomography can visualize the distribution of a plethora of molecules through the whole body as long as they are chemically combined with radionuclide agents, which emit ionizing radiation, at a resolution of the order of the millimeter. Planar X-ray imaging and tomography (sub-millimeter resolution order) capitalize on the physics of X-ray attenuation to display anatomical images of hard tissue. By using spectral techniques, soft tissue and molecular components can be resolved at the expense of using ionizing radiation. Magnetic resonance infrared (resolution of the order of the millimeter) leverages the relaxation properties of the spin of nuclei to show images with rich versatile soft tissue contrast, however, label-free molecular imaging is challenging. Moreover, the cost of this technology is tremendous, preventing its massive use beyond large hospitals and clinics. Pure US imaging (resolution ranging from tens of micrometers to few hundred micrometers depending on depth) generates contrast based on the reflection of sound mainly at tissue interfaces, leading to useful morphological images, but offers no molecular information. Finally, standard optical methods using regular optical cameras can only image at high resolution (sub-micrometer range) at shallow depths (<1 mm). Beyond, those depths images become completely blurred due to photon scattering, and no structures are visible.

1.1. Imaging Modes: Single-Wavelength vs Multi-Spectral Imaging

OAI systems can be utilized using a single-wavelength or several wavelengths for illumination. Single-wavelength illumination leads to images that display the distribution of the bio-compounds that absorb more efficiently this specific wavelength. For example, in the visible range and near infrared (from 420 to 900 nm) OAI produces images whose contrast is related to the concentration of melanin and oxy/deoxy hemoglobin. When moving into the short-wave infrared region (up to 1400 nm) the contribution of water, proteins, and lipids to signal overcome by orders of magnitude the contribution of melanin and hemoglobin [7]. Importantly, the contribution of each of the compounds to the signal is mixed. Therefore, one knows that the intensity of voxels of the images is related to the concentration of these compounds but cannot infer information about their relative concentration.

On the other hand, multi-wavelength illumination allows to retrieve the concentration of each specific compound. In this imaging mode, usually referred as multi-spectral optoacoustic tomography (MSOT) or spectral photoacoustic tomography, the tissue is illuminated with different wavelengths obtaining one image per wavelength. From the resulting set of images an optoacoustic spectrum can derived for each pixel, finding the concentration of each compound through spectral unmixing algorithms. Nevertheless, from a mathematical perspective, the unmixing problem represents a considerable challenge since after few millimeters deep in tissue, the spectra of each of the compounds become indistinguishable [8,9].

1.2. Operational Classification of Optoacoustic Modalities

OAI modalities can be classified in two groups using an operational criterion which, in turn, is related to the penetration-to-depth ratio imposed by the physics of US: macroscopy and mesoscopy (Table 1).

Macroscopic implementations are well suited for performing molecular imaging at the organ level, with a resolution of ~200 μm at depths up to 5 cm. Macroscopic OAI modalities have found a large variety of potential applications in numerous medical specialties including endocrinology, oncology, cardiology, dermatology, rheumatology or pediatrics.

 doi:10.20944/preprints202404.1202.v2

Mesoscopic implementations are well suited for molecular imaging at the tissue level, at a resolution of ~10-100 μm and depths up to 5 mm. Mesoscopic OAI modalities have found several potential applications in dermatology, oncology, cardiology and endocrinology.

For the sake of completeness, it is necessary to mention the microscopic domain. In microscopic systems, resolution is generally governed by optical diffraction instead of US diffraction at the expense of a very low penetration depth (several micrometers). This domain is prescribed for the medical operator interested in observing single cells at the surface of tissue. Therefore, it is finding applications in histological analysis that are beyond the scope of this review paper.

Table 1. Technical and operational characteristics of optoacoustic mesoscopy and macroscopy (green color) within their medical specialties in a format recognized in the European Union and European Economic Area (orange color).

	Optoacoustic Mesoscopy	Optoacoustic Macroscopy
Bandwidth	10-200 MHz	<10 MHz
Lateral Resolution	<100 μm	100-500 μm
Axial Resolution	10-100 μm	100-500 μm
Depth	0-10 mm	>10 mm
Medical Specialty	Cardiology, Dermatology, Endocrinology, Hematology, Oncology, Pathology, Plastic Surgery, Rheumatology	Cardiology, Dermatology, Endocrinology, Gastroenterology, General Surgery, Hematology, Inmunology, Neurology, Obstetrics and Gynaecology, Oncology, Orthopaedics, Pathology, Paediatrics, Podiatry, Rheumatology, Urology, Vascular Surgery

1.3. Macroscopic Systems

In order to image macroscopic structures (vessels, distribution of fat or proteins, etc.) at the organ level, OAI systems operate using US detectors with acoustic parameters similar to those of the US systems commonly used in the clinic (central frequency and bandwidth <10 MHz).

In a common approach, macroscopic implementations tend to merge standalone US imaging systems with OAI devices. This format offers three advantages: 1) the same US array can be used for OAI and US data acquisition; 2) the complementary nature of the information given by each sub-system may expedite clinical applications; 3) by providing familiar anatomical US images a positive attitude of the medical practitioner towards the new technology is created.

Generally, two approaches can be taken when designing such systems. In approach A linear arrays are used (Figure 1a). In approach B curvilinear arrays formed by cylindrically focused transducers are used (Figure 1b). In the former, high quality US images can be obtained at the expense of a reduced quality in the OAI images. Such quality mismatch is explained by the coherent nature of the optoacoustic wave's generation as opposed to the random nature of US reflection in tissue [10]. For similar reasons in approach B high quality optoacoustic images are obtained at the expense of a reduced quality in the US images. The larger the aperture covered by the detectors around the imaged object the higher the quality of the optoacoustic reconstructions. Both approaches lead to 2D images that display tissue up to 5 cm deep.

Another common macroscopic approach consists of utilizing semispherical arrays (Figure 1c). Such arrays can achieve 180º aperture leading to 3D images. In several embodiments the semispherical array is located under a bed and scanned on a 2D grid below the imaged object to obtain 3D images of large field of views. Alternatively, the array can be scanned mechanically or manually around the imaged location.

 doi:10.20944/preprints202404.1202.v2

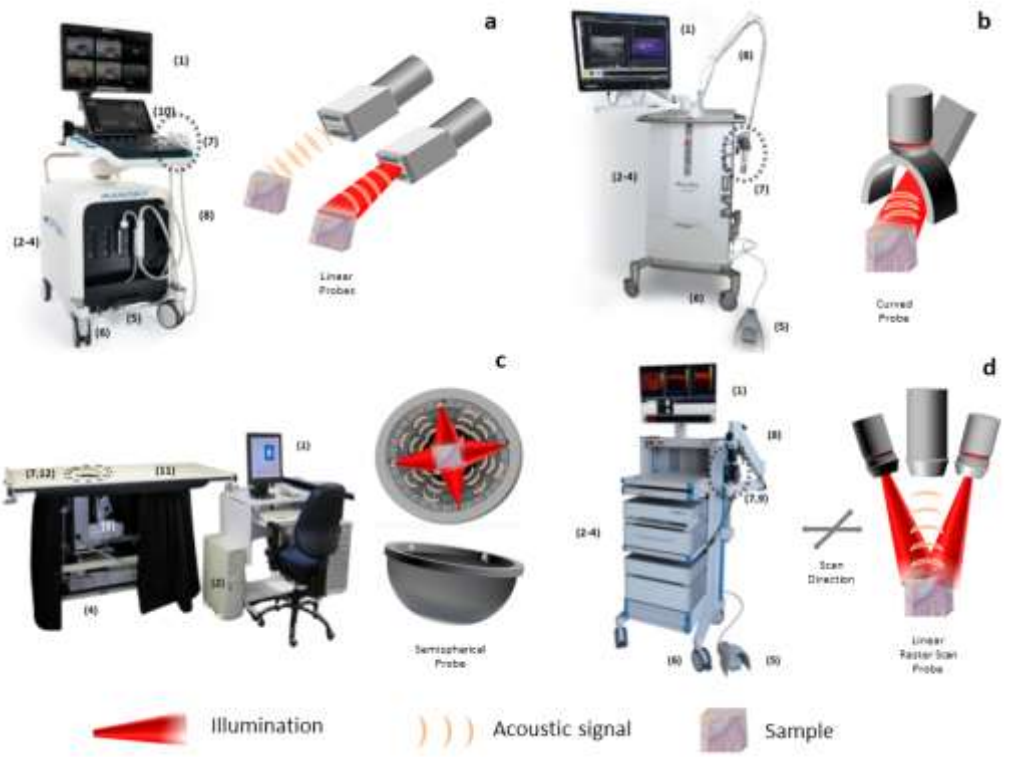

Figure 1. Schematics of the representative implementation of OAI corresponding to commercial systems used for clinical applications. (a) Commercial breast imaging system Imagio with linear array - FDA approval, first CE Mark approval - for clinical research from Seno Medical Instruments. (b) Multi-spectral optoacoustic tomography Acuity with curvilinear array for clinical research from iThera Medical. (c) Multi-modality medical imaging optoacoustic mammography with semispherical array of the University of Twente. (d) Raster-scan optoacoustic mesoscopy Explorer C50 for clinical research from iThera Medical. Each system is equipped with a different probe. System components: (1) display monitor, (2) operating PC, (3) data acquisition device, (4) laser light source, (5) foot switch, (6) wheel lock, (7) probe, (8) flexible arm, (9) scanning stage, (10) touch screen, (11) bed unit, (12) aperture for semispherical detector array.

1.4. Mesoscopic Systems

Typical mesoscopic systems are based on epi-illumination of tissue and detection of optoacoustic signals at locations along a line or a 2D-dimensional grid on the skin surface. To be able to image structures at the tissue level (micro-vasculature, cells, etc.), the detector must operate in frequency regions well above 10 MHz. Large bandwidths (up to 100 MHz) are required to achieve an axial resolution of ~10 μm. Usually, a single detector is scanned to capture OAI signals along the line or grid (Figure 1d), in a configuration that is called raster-scan optacoustic mesoscopy (RSOM). Multi-element arrays can also be employed as alternatives to single-element detectors. These are most of the times high frequency linear arrays or high frequency semispherical arrays. However, mesoscopy based on single-detectors generally offers superior imaging performance compared to multi-element arrays, since larger bandwidths can be achieved [1].

1.5. Endoscopy

OAI has been implemented in the form of endoscopic systems for imaging the esophagus, the prostate, the vaginal walls, or the lumen of vessels [11–15]. The variety of such systems would require a distinct review. Therefore, they are beyond the scope of this document.

2. Review Studies

 doi:10.20944/preprints202404.1202.v2

In what follows, we review the essential literature about the clinical studies carried out in approximately the last 10 years using OAI technology in clinical medicine with human in-vivo experiments. We will differentiate the medical domain and its associated applications, the class to which the OAI system belongs (macroscopy or mesoscopy), whether the study is registered in a national/international database of clinical records and the certification level of the system (if any at all). For each medical field, we briefly explain why OAI may have an impact in the clinic.

2.1. Macroscopic Systems

2.1.1. Cancer Imaging

OAI systems carry a highly competitive edge over other imaging technologies for cancer monitoring, diagnosis and therapy guidance [16,17]. The advantage stems from the fact that OAI is very well suited for resolving the vascular architecture, going well beyond the capabilities of standalone US imaging systems. Moreover, it does not have the cost disadvantages of magnetic resonance infrared and the safety issues of computed tomography and positron emission tomography. For example, it has been shown that small vessels (diameter <1 mm [18]) cannot be resolved by Doppler US while OAI is capable of visualizing them. Hence, aberrant vessel growth typical from malignant lesions can be displayed by OAI systems with better fidelity than US systems.

The outstanding abilities of OAI to image vessels results from a fortuitous combination of the magnitudes of several parameters like the sensitivity and bandwidth of today's US transducers, the maximum laser energy permitted in tissue, tissue acoustic properties, size of the vessels and tissue optical properties. It is worth noting that the optical absorption coefficient (μ_a) (Figure 2) of hemoglobin in the visible and near infrared range is orders of magnitude higher than the optical absorption of the surrounding biomolecules. Since the strength of the OAI signal is directly proportional to μ_a, OAI systems display vascular structures with virtually no background noise.

OAI not only depicts the vascular architecture but can also resolve the concentration of oxy/deoxy hemoglobin at high resolution when implemented as MSOT [8,9]. Therefore, the oxygenation status of vessels can be calculated, information which may be used for functional imaging (while the patient performs a specific action, for example), or to detect metabolic abnormalities related to tumor malignancy. Nevertheless, the inverse problem that has to be solved to calculate the oxygenation values is challenging due to ill-posedness issues [8,9].

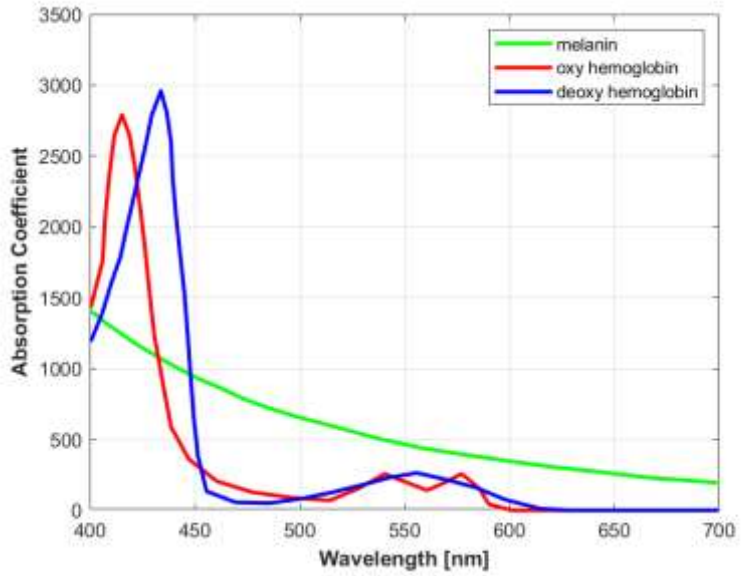

Figure 2. Optical absorption coefficient of different chromospheres in the visible spectral range: oxy/deoxy hemoglobin and melanin [19].

 doi:10.20944/preprints202404.1202.v2

We refer first to the imaging system from Seno Medical Instruments called Imagio, since it has been the first to obtain the FDA approval for breast cancer imaging [20]. The system combines OAI and US using a linear array (Figure 1a and section "Macroscopic system implementations") and can now be used in the clinic to increase the accuracy of categorization of breast tumors. Seno Medical Instruments performed a series of pivotal clinical studies to establish a reasonable assurance of safety and effectiveness of the Imagio system to achieve the positive outcome of the FDA evaluation. The multi-center clinical trial (NCT01943916) played a central role as primary clinical study. Several articles have been published following this study [21–23], demonstrating that the system can obtain functional and anatomical maps of the vasculature of breast masses (Figure 3a). Other researchers have explored the additional benefit of OAI in optimizing categorization of breast masses during US examinations [24–26].

Many other systems have been investigated for breast cancer imaging. The OAI system developed by Canon Inc based on a semispherical array (Figure 1c) has been used at least in five studies from a team of the Kyoto University. In the work presented in [27] the authors used the so called PAI-01 to image 27 breast tumor lesions, including 21 invasive breast cancers, 5 ductal carcinomas in-situ, and one phyllodes tumor. The system detected the lesions in 15 out of 21 cases. The same system was used in [28] to study tumor vessel distribution and oxygen saturation in 57 patients with breast cancer. The study was included in the clinical trials registry of the University Hospital Medical Information Network of Japan with register ID (UMIN000003406). The results demonstrated the potential of the system for identifying malignant functional features of breast tumors. A modified version of the PAI-01 system (PAI-03) was applied to image breast cancer in 30 patients evaluating oxygen saturation and tumor-related vascular structures obtaining higher penetration depth [29]. PAI-03 was used in [30] to count vascular branching points as a potential biomarker for breast cancer in 30 patients enrolled in clinical trial (UMIN000012251). Tumor-related vessels structures around breast tumors (Figure 3b) were visualized in [31] with a new version of the system called PAI-04. A total of 190 patients participated in the study under clinical trials (UMIN000018893, UMIN000022215 and UMIN000022767).

The University of Twente developed a multi-modality optoacoustic medical imaging mammoscope [32] based on a semispherical array to study breast cancer. The authors in [33] visualized breast malignancies in 29 patients included in the Netherlands clinical trial (TC2945) approved by the institutional review board (IRB) of the Medisch Spectrum Twente Hospital. The same system and data were used in [34,35] to capture breast cancer malignancies related to tumor vascularity. The images were compared to magnetic resonance imaging and vascular staining in histological slices. A new version of the Twente mammoscope was used in [36] to image 3D vascular networks in healthy breasts (clinical trial TC6508). The system included a dual-wavelength laser to improve the image's contrast of hemoglobin.

A group from the University of North Carolina developed an OAI system dedicated to breast cancer imaging also based on a semispherical array from OptoSonics Inc [37]. In a pilot study, the authors demonstrated good visualization of the vasculature in the breast tissue of 4 patients. A similar system that incorporates a curvilinear array that is scanned to achieve full view was developed in Caltech Optical Imaging Laboratory (COIL) in California [38,39]. The data acquisition speed was high enough to achieve single-breath-hold imaging, avoiding artifacts due to motion. The system was able to capture images with detailed angiographic information in 7 patients with breast cancer.

A team from the Institute of Biological and Medical Imaging (IBMI) in Munich developed a hybrid OAI/US system based on a hand-held curvilinear array called the Acuity system (Figure 1b). Importantly, this system, which is commercialized by Ithera Medical, obtained the CE mark for clinical research. The system has been tested in a couple of clinical studies related to breast cancer. More specifically, the IBMI team used the Acuity system on 13 patients [40]. The spectral range of the platform allowed the computation of oxy/deoxy hemoglobin, total blood volume, lipid and water. In the work presented in [41], using images obtained from 22 patients with breast cancer, the authors derived markers of malignancy, including vasculature abnormalities, hypoxia, and inflammation. The study was approved by the IRB of the Technical University of Munich (Nº 27/18 S).

 doi:10.20944/preprints202404.1202.v2

Another team from IBMI developed a system based on a semispherical array and tested its performance for in-vivo imaging of breast cancer [42]. The authors could identify vascular structures and the distribution of oxy/deoxy hemoglobin and total hemoglobin operating the system in a hand-held fashion.

A portable OAI breast cancer system based on two linear arrays that are scanned on top of a compressed breast was developed in [43] at the University of Buffalo. The results showed images of the breast in craniocaudal plane, a viewpoint that is most recognizable to radiologists and is simple to understand.

The Laser Optoacoustic Ultrasonic Imaging System Assembly (LOUISA) system from TomoWave Laboratories Inc [44], which is based on a rotating semispherical array (Figure 1c), has been also used for morphological and functional vascular imaging of the human breast. The study was approved by the MD Anderson Cancer Center.

Thyroid cancer has been one of the main targets of the clinical studies performed with OAI technology. The superficial location of the thyroid gland makes it very convenient to be imaged with OAI. The Acuity system was used by an IBMI team [45] to evaluate benign and malignant thyroid disorders including Grave's disease and thyroid nodules in 18 patients. The same team in collaboration with the University of Groningen used the system in 50 patients enrolled in clinical trial (NCT04730726). The authors found features associated with vasculature patterns in thyroid nodules suspicious for malignancy [46].

A group from Pohang University of Science and Technology (POSTECH) developed a hybrid OAI/US imaging system formed by an US commercial FDA approved system, a laser, and a customized linear array [47]. The system was used to image 52 patients included in clinical trial (NCT00170196). Results demonstrated real-time OAI/US imaging capabilities of thyroid nodules in-vivo in 29 benign cancer lesions and 23 papillary thyroid cancers.

A team from Peking University [48] modified a linear array from a commercial clinical US platform to perform OAI. The system was used to study suspicious malignant thyroid nodules with indications for fine needle aspiration biopsy and histology [2]. OAI images confirmed the diagnosis in 13 patients with thyroid cancer. The research was performed under approval from the IRB of the Peking Union Medical College Hospital.

Macroscopic OAI systems have also been used for imaging skin cancer. The group from IBMI in collaboration with the National Skin Center of Singapore [49] used the Acuity system to image 3 patients showing structural and functional 3D mapping of skin tumors. A different group from the University of Duisburg-Essen [50] applied the Acuity system to evaluate the metastatic status of sentinel lymph nodes in skin melanoma. A total of 20 patients included in the German clinical trials register (DRKS00005447) were imaged. Results indicated that the system's technology using ICG as contrast agent was able to detect sentinel lymph nodes up to 5 cm depth. Last but not least, the system created at POSTECH was used in [51] to image different types of melanomas in-vivo in 6 patients provided depth, size, and metastatic type.

2.1.2. Cardio-Vascular Imaging

As explained at the beginning of the previous section, OAI is particularly well suited for imaging blood vessels, being able to resolve their oxygenation status as well. Therefore, a large amount of research effort has been oriented towards cardio-vascular imaging. Additionally, the ability of OAI to resolve other biomolecules like lipids or collagen may be useful, for example, detecting and determining the status of atherosclerotic plaques.

Several studies have been conducted by teams from IBMI using the Acuity platform. In [52] they used the system to investigate the vasculature and morphology of peripheral nerves in 12 subjects. The results linked the endogenous contrast of hemoglobin and collagen with the perfusion of connective tissue. The Acuity was applied as well for imaging atherosclerotic plaques in the carotid artery. They could relate the lipid and hemoglobin content of the plaque with its stability [53,54]. In a different study, another group from IBMI in collaboration with the University Hospital of Muenster [55] explored the potential of OAI images to diagnose congenital vascular abnormalities

 doi:10.20944/preprints202404.1202.v2

(arteriovenous malformation and venous malformation) [56]. The results revealed higher oxygenated hemoglobin levels in arteriovenous malformation than in venous malformation, providing a potential intrinsic biomarker to distinguish both conditions. In other research work in collaboration with the University Medical Center Groningen, they explored the potential of the Acuity system to predict plaque instability [57,58] in 5 patients with a symptomatic carotid stenosis. Other works studied morphological and anatomical vascular structures of human thyroids in 27 patients suffering from hypothyroidism [59,60]. In the work presented in [61] Acuity was used to assess flow-mediated dilation test. Such test could be eventually used to characterize vascular endothelial dysfunction [62].

Other research groups have also used Acuity to investigate vascular anomalies. Clinical assessment of major blood vessels and micro-vasculature in the lower limbs identifying pulsation in arteries during imaging was proposed in [18]. The research was carried out at a group from IBMI in ten human volunteers included in the Dutch national trial registry (NTR4125).

Several studies have been reported from a team of Kyoto University using the OAI platform developed by Canon Inc. The PAI-03 system ability to unravel the vascular anatomy of the thigh was explored in [63]. The system was used to identify anterolateral thigh perforators [64] and the branching patterns in the subcutaneous layer. The study included 5 patients in a registered clinical trial (UMIN000018893). The same team used the PAI-03 in [65] to analyze the vascular morphology of 23 subjects. They observed increased blood vessel curvature and arterial tortuousness with age. In a different study, they observed the vascular structures in hand and foot of smokers [66]. The images of 21 patients included in clinical trials (UMIN000018893, UMIN000022767) obtained with PAI-03 and PAI-04 revealed different functional and morphological structures in smokers compared to non-smokers.

In [67] an OAI system based on a semispherical array called 1k3D-PACT from the COIL group in California was applied in 4 patients who had a hemicraniectomy [68] to quantify oxygen saturation and blood volumes in the brain. The OAI/US system developed at POSTECH was used in [69] to visualize morphologic and physiologic features of the human foot of 6 subjects approved by the IRB (PIRB-2020-E019). Results showed the structure of the vasculature in the skin, providing functional information of hemoglobin, oxygen saturation, vessel density, and vessel depth up to 10 mm. In this case, the authors used a macroscopic system for a mesoscopic application. The same system with a new semispherical array was used in [70,71] to obtain high quality imaging of the vasculature of the human forearm.

A team from IBMI [72] developed an OAI/US prototype system that combines a linear and a curved transducer array. The platform enabled the acquisition of high quality anatomical and functional information on blood oxygenation status. In the work presented in [73] an OAI system that relies on an US sensor based on a Fabry Perot interferometer developed at the University College London was used to visualize vasoconstrictor capillary beds on peripheral limbs and the dorsal artery. Fifteen patients were included in the study (IRB 1133/001). After cold water immersion, the images showed smaller vascular structures than the images obtained from subjects that were not immersed in water.

A clinical hand-held system based on a linear array developed at POSTECH was used to image the vasculature of blood vessels and hemoglobin oxygen saturation of different parts of 4 human subjects in [74]. The so called “LightSpeed” system was created at IBMI to analyze angiography of the human wrist with images displaying structures up to 5 mm deep [75]. This system includes a pulsed laser diode and a semispherical array. In [76] a system mounted with a compact tunable laser and an US linear array developed at the Center for Biomedical Engineering of the University of Texas Medical Branch was used for brain oxygenation monitoring.

There has been also works to study the vascular changes caused by diabetes mellitus using OAI platforms. For example, a research group from the University of Electronic Science and Technology of China in collaboration with the University of South Florida [77], built an OAI system to investigate hemodynamic changes of foot vessels during vascular occlusion in 14 diabetic patients. Results showed difference in the peripheral hemodynamic response when comparing healthy subjects with those suffering diabetes.

 doi:10.20944/preprints202404.1202.v2

2.1.3. Lymphatic System Imaging

Many studies have been conducted to establish the possible clinical impact of OAI in the visualization of lymphatic vessels motivated by the fact that OAI can resolve ICG, which is used for sentinel lymph node detection and other procedures.

Several research efforts from a team at the Keio University School of Medicine were devoted to applying the PAI-05 to obtain images of the lymphatic system. The authors in [78] compared the images obtained with OAI and near infrared optical imaging of the lymphatic vessels in the lower limbs of 15 subjects using ICG, demonstrating that OAI obtained a more detailed 3D representation of the lymphatic vessels. A human lymphatic pump was observed using ICG contrast and OAI in [79], where the lymphatic fluid did not flow continuously. The study was included in the Japan registry of clinical trials (JRCTs032180204). Other research efforts [80] were oriented to study the effect of aging on the lymphatic vessels in the lower leg of 19 subjects enrolled in the clinical record of [79], concluding that the number of lymphatic vessels increased with age (Figure 3c). In [81] the team evaluated the surgical procedure called lymphaticovenular anastomosis [82] using the system with a new implementation for OAI lymphangiography. The study was carried out before and after the intervention in 3 patients with lymphedema.

2.1.4. Musculoskeletal Imaging

Musculoskeletal imaging can highly benefit from the vascular imaging capabilities of OAI but also from the ability of imaging other biomolecules like collagen.

The Acuity system has been employed in different studies for diagnosis and monitoring of musculoskeletal diseases. Twenty patients with Duchenne muscular dystrophy [83] included in the clinical trial (NCT 03490214) were imaged by a group at the Friedrich Alexander University [84]. The system was applied for visualization and quantification of collagen content as an imaging biomarker for the disease.

In the work presented in [85,86] a group from IBMI imaged muscle perfusion and oxygenation under arterial and venous occlusion after exercise. The results clearly showed hemodynamic and oxygenation changes in the skeletal muscle in 4 subjects. A group from Friedrich Alexander University [87] used the system to visualize and quantify muscle wasting in pediatric spinal muscular atrophy [88]. Results from 20 patients enrolled in clinical trial (NCT04115475) showed moth-eaten optoacoustic signal patterns (Figure 3d).

An exploratory analysis to differentiate cortical from cancellous bone for spinal surgeons of a human vertebra was made at the Johns Hopkins University [89]. The platform used for the study includes a Phocus mobile laser (Opotek, USA) and a linear array. Results indicated that signals from the cortical bone have higher amplitudes than signals from the cancellous bone. In [90] a team from the University of Electronic Science and Technology of China in collaboration with University of South Florida developed an OAI system made with a tunable pulsed laser and an US curvilinear array. The system was used to track the hemodynamic changes in 6 forearm muscles during cuff occlusion. The study was approved by the IRB of the University of Chongqing.

2.1.5. Gastrointestinal Imaging

Inflammatory gastrointestinal conditions like Crohn's disease are generally characterized by angiogenesis and vasodilation in the intestinal walls. Such perturbation can be observed by OAI systems overcoming the disadvantages of intrusive endoscopes.

Acuity has been applied in several experiments involving inflammatory Bowel disease [91] in research conducted by groups from Friedrich Alexander University. The platform was used in clinical trial (NCT02622139) that included 344 patients to perform trans-abdominal evaluation of intestinal inflammation in patients with Crohn's disease [92–94]. Results suggested that hemoglobin levels in the intestinal wall have the potential to be used to differentiate between active and non-active disease (Figure 3e). In [95] data from 44 patients included in the same clinical trial was used to evaluate the

 doi:10.20944/preprints202404.1202.v2

presence and severity of ulcerative colitis [96]. The system enables assessment of disease activity and provides quantitative measurements of hemoglobin and oxygen saturation.

A novel approach to study the functional assessment of the gastrointestinal tract using ICG as a contrast agent was proposed in [97]. Ten subjects included in clinical trial (NCT05160077) were examined on two days. In day one they received standard meals and in day two standard meals plus ICG intakes. Results indicated the technical and clinical feasibility of Acuity with contrast enhanced for functional imaging of the intestine. The system was applied in [98] to study the human intestine during postprandial gastrointestinal blood flow in same patients. Results showed physiological alterations on the human intestine.

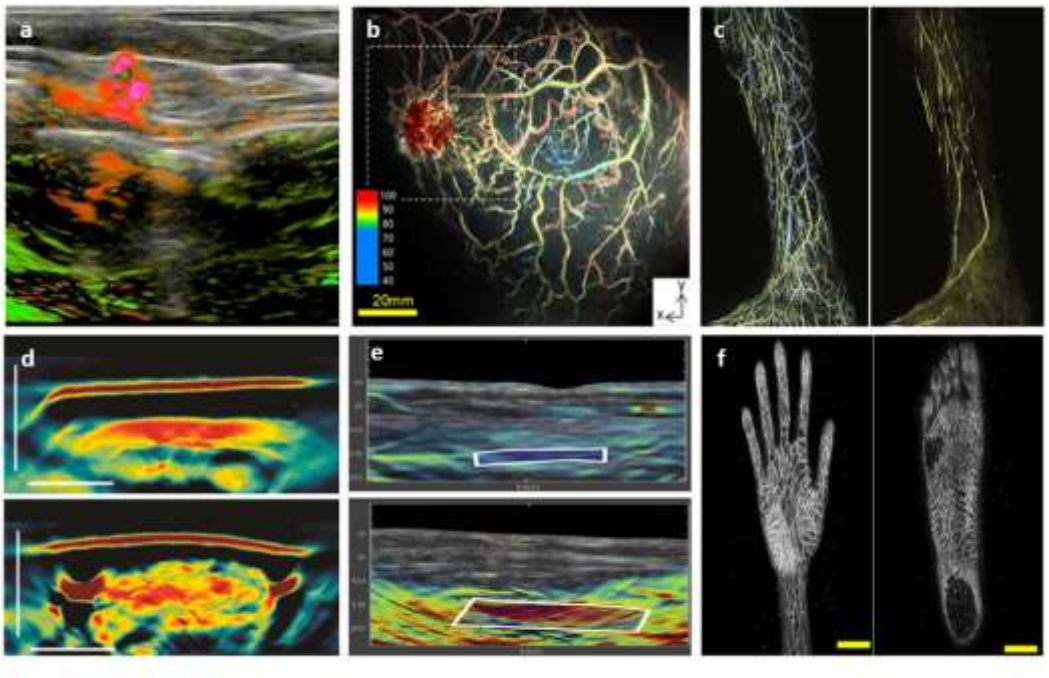

Figure 3. Optoacoustic images corresponding to several macroscopy applications. (**a**) Image of breast carcinoma acquired with the system Imagio from Seno Medical Instrument in a patient with breast cancer included in clinical trial (NCT01943916) [23]. Significant blood hypoxia and dense angiogenesis micro-vasculature (green) is shown with significant deoxygenation (red). (**b**) Image obtained from a breast cancer patient with PAI-04 platform from Canon Inc under clinical trials (UMIN000018893, UMIN000022215 and UMIN000022767) [31]. The white cubed confined the tumor colored in red. Several clustered fine blood vessels are observed in the vicinity of the tumor. The nipple at the center of this image is colored light blue because the absorption spectrum of melanin in the nipple and the spectrum of low oxygen saturation are almost the same. (**c**) Optoacoustic lymphangiography of the lymphatics vessels (yellow) and veins (blue) taking with PAI-05 under clinical trial (JRCTs032180204). Reprinted with permission from [80]. (**d**) Images of a section of the right biceps of a healthy subject (top) and a patient with spinal muscular atrophy (bottom) obtained with the system MSOT Acuity from iThera Medical under clinical trial (NCT04115475) [87]. Images show homogeneous muscle fibers in healthy volunteer, whereas patchy clusters of hypertrophic and atrophic muscles fibers lead to the moth-eaten pattern are observed in spinal muscular atrophy patient (bottom). (**e**) Images of the intestinal wall of a patient with Crohn's disease in remission (top) and active (bottom) obtained with MSOT Acuity under clinical trial (NCT02622139). In contrast with the patient remission, clinical and endoscope Crohn's disease activity is associated with increased signals for oxygenated hemoglobin (delimited with white cubes). Reprinted with permission from [92]. (**f**) Images of a palm (left) and the sole of the foot (right) obtained with the PAI-05 system. Study was under clinical trial (UMIN000022767) [108].

 doi:10.20944/preprints202404.1202.v2

2.1.6. Miscellaneous

Optoacoustic macroscopy has been also applied for imaging human inflammatory joint diseases [99]. A team from the University of Twente [100] evaluated the feasibility of using a hybrid OAI/US system to assess clinical evidence of synovitis. The authors analyzed the inflammation of proximal inter-phalangeal joints in 17 patients approved by the IRB. The system is based on a MylabOne US platform from Esaote that incorporates a diode laser and an US linear array.

A team of the University of Cambridge [101] used the Acuity system to study physiological and vascular changes in the menstrual cycle. Results in 21 patients approved by the IRB showed significant differences in image intensities for proliferative/follicular and secretory phases, the two main phases of the menstrual cycle [102]. Acuity also has been used in a group of the University of Lusofona in Portugal [103]. The system was capable of visualizing suprasystolic reactive hyperemia [104] during occlusion in ten patients. The research was approved by the corresponding IRB. Results revealed that the suprasystolic occlusion obliterated the superficial smaller vessels and evoked stasis in deeper structures.

In [105] the authors proposed to use OAI for preoperative vascular evaluation of anterolateral thigh flap. Eight patients were enrolled in the study following approval by the IRB of the Kyoto University Graduate School of Medicine (C1298). For each patient, images of the head and neck were obtained with the PAI-05 system, creating a vascular map of anterolateral thigh flap that facilitates surgeries. The same system was used in [106] to evaluate the distribution of thoracodorsal artery perforators [107] in 18 patients. Another work in collaboration with the Japan Science and Technology Agency that analyzed human limbs with PAI-05 was presented in [108]. The authors obtained high quality images of palm, thigh, and foot (Figure 3f) in 30 patients included in clinical trial (UMIN000022767).

Other studies have been performed using the Acuity system. In [109] a team from IBMI applied the system to study lipid metabolism through measurements of lipid signals in arteries, veins, skeletal muscles, and adipose tissues. Four participants approved by the IRB of the Medical Faculty of the Technical University of Munich (Nº 349/20 S) were included in the study. Another team from the University of Zurich [110] imaged 7 patients for preoperative mapping and selection of incision sites for surgery.

2.2. Mesoscopic Systems

OAI mesoscopy systems operate at the tissue level, being able to reach several mm deep preserving high resolution (tens of micrometers). Such imaging performance is particularly well suited for visualizing the micro-vasculature in the skin (the dermal vessels diameter ranges from 10 micrometers to 100 micrometers [111]). In fact, when operating using ultra-wideband transducers, OAI mesoscopy is able to reveal the dermal micro-vasculature with a fidelity which is not accessible to other technologies [111]. The skin vessel structure plays an essential role in the pathogenesis of most dermatological conditions but also in cardio-vascular and metabolic diseases. Hence, OAI mesoscopy opens many clinical research opportunities in several medical fields.

A clinical hybrid OAI/US mesocopy system based on a low energy solid state laser was developed at Fraunhofer Institute for Biomedical Engineering [112]. The system was able to provide images of the morphology of the subcutaneous micro-vasculature by raster scanning a spherically focused transducer.

A group from the University of Electronic Science and Technology of China [113] designed a mesoscope based on a high frequency semispherical array, and assessed its potential to monitor hemodynamic changes in foot vessels. Results from 12 human subjects showed the decline in micro-vascular function with age.

A multi-modality system combining OAI mesoscopy and optical coherence tomography for skin imaging was developed at the Center for Medical Physics and Biomedical Engineering of the University of Vienna in collaboration with the University College London [114]. The system was able to display the micro-vascular anatomy of the different layers of the skin of the human palm at depths up to 5 mm. A similar system was used [115] to study different dermatological pathologies. Results

 doi:10.20944/preprints202404.1202.v2

provided information about tissue morphology and vasculature (Figure 4a–c) of 24 patients with different types of eczema. The research was approved by the IRB of the Medical University of Vienna.

In the work presented in [116] a team from IBMI developed an RSOM system to image human skin that revealed comprehensive views of the skin micro-vascular structure. Such views included the smallest capillary loops that are close to the skin surface and the arterioles and venules of the deep dermis. Since then, different versions of the system have been developed by several IBMI teams. Their potential for impacting the clinical routine of different dermatological, cardio-vascular and metabolic diseases has been assessed. In [117] the group applied the RSOM system to visualize the micro-vascular structure of the nail folds. Six healthy volunteers participated in the study. RSOM was able to provide the capillary loop density and diameter which are two parameters involved in systemic sclerosis. In [118] the authors developed an RSOM system capable of capturing the skin micro-vascular hyperemic response to cuff, with potential implications in the assessment of endothelial dysfunction. The RSOM images showed clear functional differences between smokers and non-smokers. The same group has also been exploring the ability of RSOM for the assessment of changes in the dermal micro-vasculature in diabetic patients [119] (Figure 4d-4f). A total of 92 human subjects were enrolled in the experiment under approval from the IBR of the Hospital of the Technical University of Munich. In [120,121] an RSOM system incorporating multi-spectral capabilities was used to calculate the distribution of oxy/deoxy hemoglobin and melanin in the skin.

The same IBMI group explored in [122] the possibility of using RSOM to improve allergic patch testing, enrolling a total of 60 patients. Results suggested higher fragmentation of skin vasculature in allergic skin reactions. Similarly, the system was applied in [123] to quantify skin sensitivity to ultraviolet light in 7 subjects, revealing the microscopic vascular effect of the erythematous skin reaction [124] after exposure to ultraviolet light. Berezhnoi et.al. [125] applied RSOM to monitor heat-induced hyperemia in 6 subjects. Results showed increased total blood volume in the skin in response to local heating at single-micro-vessel resolution in the forearm. Omar et.al. [126] combined RSOM with machine learning techniques identifying morphological characteristics of skin lesions. In [127] it was shown that RSOM is capable of visualizing skin morphology and vascular patterns in psoriasis patients. The work was extended in [128] revealing inflammatory and morphological skin features that indicated treatment efficacy with sensitivity, accuracy, and precision not accessible to standard clinical metrics. All the above studies were approved by the IRB of the Faculty of Medicine of the Technical University of Munich.

A team from IBMI [129] applied an OAI mesoscope based on a semispherical array to measure the structural and physiological features of intact hair follicles and pilosebaceous units. The research was carried out with 7 healthy volunteers included in clinical trial (DSRB 2014/00677). In [130] the National Skin Center of Singapore in collaboration with another team from IBMI used RSOM Explorer C50 system for clinical research from iThera Medical (Figure 2d). A total of 91 patients with atopic dermatitis enrolled in the study with the approval from the IRB of the National Health Group of Singapore (Nº 2017/00932). Results demonstrated significant differences between healthy and atopic dermatitis patients in terms of epidermis thickness, total blood volume and the ratio of low frequency and high frequency signals in the dermis.

 doi:10.20944/preprints202404.1202.v2

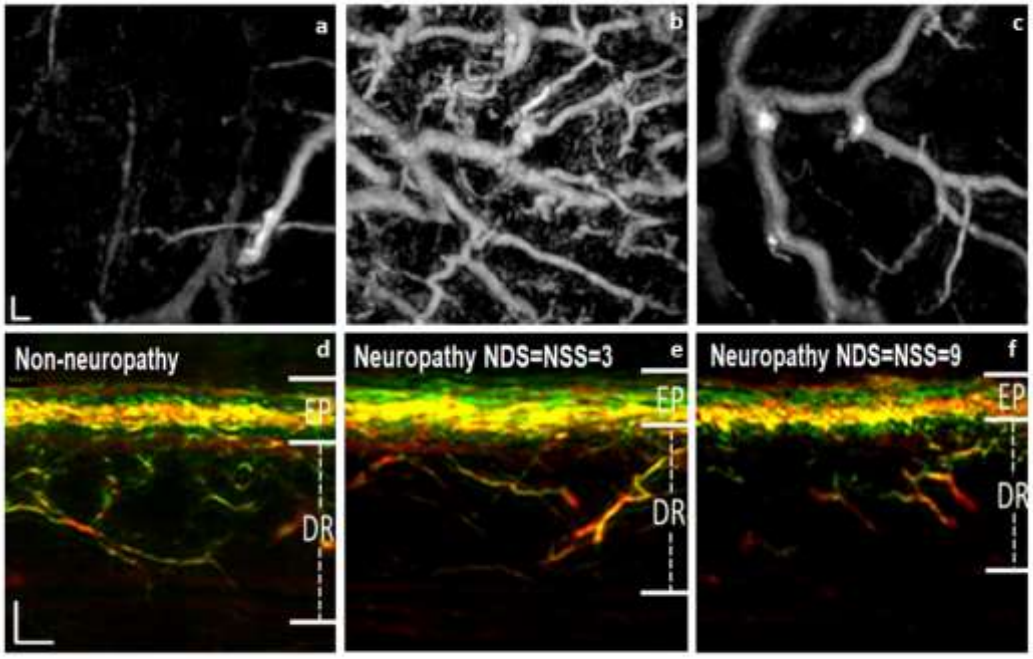

Figure 4. Optoacoustic images corresponding to several mesoscopy applications. (**a-c**) Mesoscopic images approved by the University of Vienna of a healthy subject (a), a patient with chronic hyperkeratotic hand eczema (b), and a patient with the disease under treatment (c) [115]. The depth range between 1.2 and 3.0 mm includes vessels of the deep vascular plexus in the dermis (DR) as well as few vessels of the subcutaneous fat. Note the hypervascularization in the patient (b) and how because of the antiproliferative and vasoconstrictive effects of the topical steroid used, the vascular network is sparse (c). (**d-f**) Cross-sectional images of skin in 3 diabetic patients with different neuropathology scores (neuropathy disability score (NDS) [131] and neuropathy symptom score (NSS) [132]) produced with a custom-made RSOM system under approval from the hospital of the Technical University of Munich. The DR and epidermis (ER) are delimited with white bars. Figure d shows result for a patient without neuropathology, figure e for a patient with low neuropathology scores, and figure f for a patient with high neuropathology scores. It is observed that as the neuropathology score increases, there is a decrease in the thickness of the DR and ER, being more visible in the DR [119]. Scale bar = 500 μm.

3. The Path towards Clinical Translation: Are We Close to Clinical Adoption?

Assuming that funding is not a problem, the development and commercialization of new medical devices is a long and complex process (on average it takes 3 to 7 years from proof-of-concept to regulatory approval in the USA) [133]. The teams committed to translate new technologies into medical devices engage on a trip full of uncertainties and challenges that, on many occasions, may end up in failure. Apart from the scientific and technical challenges related to redesign and testing of the technology until a viable device is ready for end-users (which usually takes 2 to 3 years and costs of a few million euros [134]), the team must overcome numerous regulatory barriers, which may be especially stringent with most innovative technologies.

Regulation imposes different legal, technical, and clinical requirements, which need to be considered from the very beginning of the design process. For example, devices must be designed in compliance with highly restrictive electrical safety and electromagnetic compatibility requirements, since these must be certified by an accredited lab before any clinical test relevant for regulatory approval can be performed. These clinical tests must also be pre-approved by regulatory authorities and by the ethics and scientific committees of the center(s) performing the tests, which may require

 doi:10.20944/preprints202404.1202.v2

several iterations until the study can even start. Furthermore, medical device regulations apart from changing in time and vary from country to country, may require, depending on the device classification, and continuous surveillance of any relevant data. Additionally, they require periodic audits by different regulatory authorities, maintenance of considerable amounts of documentation. Moreover, the deployment of measures and establishment of protocols intended to ensure different aspects of the quality and safety of the devices are needed. Consequently, apart from the budget required for initial regulatory approval, there will be non-neglectable regulatory costs during product lifetime which must also be considered when evaluating the viability of any business model related to the medical device.

Despite of the wealth of casuistry, there are a few steps on the approval process for new medical technologies that are common in most regulatory frameworks. Initially, devices are classified according to their risk level for the patient and, depending on this risk, the testing requirements are established. By default, medical devices using new technology will be classified in the highest risk group and are required to undergo the most rigorous reviews that include provision of exhaustive clinical evidence to validate the performance and safety of the technology. Furthermore, depending on the nature of the device and its proposed use, the complexity of the clinical testing (ranging from basic studies with a limited number of patients, to large multi-center randomized clinical trials in which hundreds to thousands of patients must be recruited and followed up), can severely affect the time and cost of getting the medical device approved.

Fortunately, the clinical part of the regulatory approval process can be much simpler if there are already approved devices that have only minor differences with the device under evaluation. If such devices exist, and depending in which degree equivalence can be demonstrated (e.g., in terms of intended use, technology, performance, etc.), clinical testing requirements can be much less stringent, being determined according to the risk classification of the equivalent device. Between 2014-2021, the first medical imaging device using OA technology (Imagio, Seno Medical Instruments USA) [20] was approved by the regulatory authorities of the EU and USA, which represent the two biggest and most regulated medical device markets globally. This system, which combines standard US and OAI and is intended to evaluate breast abnormalities in adult patients, has established the basis for expanding OAI into different applications, and the introduction of new devices into the clinics.

The breakthrough achieved by the Imagio system together with the wealth of successful clinical studies performed with other systems across a wide range of clinical applications, precludes full clinical adoption of OAI in the medium term.

Author Contributions: Conceptualization, J.A.; data curation, S.C.; writing-original draft preparation, S.C., E.L., J.A.; writing-review and editing, S.C., J.R., J.A.; visualization, S.C.; supervision, J.A.. All authors have read and agreed to the published version of the manuscript.

Funding: Juan Aguirre would like to thank the financial support from the Madrid Talento grant 2020-T1/TIC-20661TEC (PRECISION).

Conflicts of Interest: The authors declare no conflict of interest.

Acronyms

IBMI: Institute of Biological and Medical Imaging
ICG: Indocyanine Green
IRB: Institutional Review Board
MSOT: Multi-Spectral Optoacoustic Tomography
OAI: Optoacoustic Imaging
POSTECH: Pohang University of Science and Technology
COIL: Caltech Optical Imaging Laboratory
RSOM: Raster-Scan Optoacoustic Mesoscopy
US: Ultrasound

 doi:10.20944/preprints202404.1202.v2

References

1. M. Omar, J. Aguirre, and V. Ntziachristos, "Optoacoustic mesoscopy for biomedicine," Nat. Biomed. Eng., Apr. 2019, doi: 10.1038/s41551-019-0377-4.
2. I. Steinberg, D. M. Huland, O. Vermesh, H. E. Frostig, W. S. Tummers, and S. S. Gambhir, "Photoacoustic clinical imaging," Photoacoustics, vol. 14, pp. 77–98, 2019, doi: 10.1016/j.pacs.2019.05.001.
3. A. Karlas, M. Pleitez, J. Aguirre, and V. Ntziachristos, "Optoacoustic Imaging in Endocrinology," Nat. Rev. Endocrinol., 2021, doi: 10.1038/s41574-021-00482-5.
4. J. Aguirre, A. Giannoula, T. Minagawa, L. Funk, P. Turon, and T. Durduran, "A low memory cost model based reconstruction algorithm exploiting translational symmetry for photoacoustic microscopy," Biomed Opt Express, vol. 4, no. 12, pp. 2813–2827, Dec. 2013, doi: 10.1364/BOE.4.002813.
5. A. Rosenthal, V. Ntziachristos, and D. Razansky, "Acoustic Inversion in Optoacoustic Tomography: A Review," Current Medical Imaging Reviews, vol. 9, pp. 318–336, 2013.
6. X. L. Dean-Ben, A. Buehler, V. Ntziachristos, and D. Razansky, "Accurate model-based reconstruction algorithm for three-dimensional optoacoustic tomography," IEEE Trans Med Imaging, vol. 31, no. 10, pp. 1922–8, Oct. 2012, doi: 10.1109/TMI.2012.2208471.
7. A. Berezhnoi et al., "Optical features of human skin revealed by optoacoustic mesoscopy inthe visible and short-wave infrared regions," Opt Lett, vol. 44, no. 17, pp. 4119–4122, Sep. 2019, doi: 10.1364/OL.44.004119.
8. S. Tzoumas et al., "Eigenspectra optoacoustic tomography achieves quantitative blood oxygenation imaging deep in tissues," Nat Commun, vol. 7, p. 12121, 30/online 2016, doi: 10.1038/ncomms12121 http://www.nature.com/articles/ncomms12121#supplementary-information.
9. B. Cox, J. G. Laufer, S. R. Arridge, and P. C. Beard, "Quantitative spectroscopic photoacoustic imaging: a review," J Biomed Opt, vol. 17, no. 6, p. 061202, Jun. 2012, doi: 10.1117/1.JBO.17.6.061202.
10. X. L. Deán-Ben and D. Razansky, "On the link between the speckle free nature of optoacoustics and visibility of structures in limited-view tomography," Photoacoustics, vol. 4, no. 4, pp. 133–140, 25 08/10/received 09/30/revised 10/13/accepted 2016, doi: 10.1016/j.pacs.2016.10.001.
11. A. Horiguchi et al., "Pilot study of prostate cancer angiogenesis imaging using a photoacoustic imaging system," Urology, vol. 108, pp. 212–219, 2017, doi: 10.1016/j.urology.2017.07.008.
12. R. Kothapalli et al., "Simultaneous transrectal ultrasound and photoacoustic human prostate imaging," Sci. Transl. Med., vol. 11, p. 2169, Aug. 2019, doi: 10.1126/scitranslmed.aav2169.
13. S. Nandy et al., "Evaluation of Ovarian Cancer: Initial Application of Coregistered Photoacoustic Tomography and US," Radiology, vol. 289, no. 3, pp. 740–747, 2018, doi: 10.1148/radiol.2018180666.
14. Y. Qu et al., "In vivo characterization of connective tissue remodeling using infrared photoacoustic spectra," J. Biomed. Opt., vol. 23, Dec. 2018, doi: 10.1117/1.JBO.23.12.121621.
15. Y. Li, G. Lu, Q. Zhou, and Z. Chen, "Advances in Endoscopic Photoacoustic Imaging," Photonics, vol. 8, no. 7, 2021, doi: 10.3390/photonics8070281.
16. Y.-S. Chen, D. Yeager, and S. Y. Emelianov, "Chapter 9 - Photoacoustic Imaging for Cancer Diagnosis and Therapy Guidance," in Cancer Theranostics, X. Chen and S. Wong, Eds., Oxford: Academic Press, 2014, pp. 139–158, doi: 10.1016/B978-0-12-407722-5.00009-8.
17. Lin, Li and Wang, Lihong V, "The emerging role of photoacoustic imaging in clinical oncology," Nat. Rev. Clin. Oncol., vol. 19, no. 6, pp. 365–384, 2022, doi: 10.1038/s41571-022-00615-3.
18. A. Taruttis, A. C. Timmermans, P. C. Wouters, M. Kacprowicz, G. M. van Dam, and V. Ntziachristos, "Optoacoustic Imaging of Human Vasculature: Feasibility by Using a Handheld Probe," Radiology, vol. 281, no. 1, pp. 256–263, 2016, doi: 10.1148/radiol.2016152160.
19. R. Akaho, M. Hirose, and N. Tsumura, "Evaluation of the robustness of estimating five components from a skin spectral image," Opt. Rev., vol. 25, pp. 181–189, 2018, doi: 10.1007/s10043-017-0402-3.
20. "Premarket Approval Imagio Breas Imaging system." Accessed: Nov. 01, 2023. [Online]. Available: https://www.accessdata.fda.gov/scripts/cdrh/cfdocs/cfpma/pma.cfm?id=P200003.
21. J. Zalev et al., "Clinical feasibility study of combined opto-acoustic and ultrasonic imaging modality providing coregistered functional and anatomical maps of breast tumors," in Photons Plus Ultrasound: Imaging and Sensing 2013, A. A. Oraevsky and L. V. Wang, Eds., SPIE, 2013, p. 858103. doi: 10.1117/12.2009112.
22. J. Zalev et al., "Opto-acoustic breast imaging with co-registered ultrasound," in Medical Imaging 2014: Biomedical Applications in Molecular, Structural, and Functional Imaging, R. C. Molthen and J. B. Weaver, Eds., SPIE, 2014, p. 90381J. doi: 10.1117/12.2043050.
23. A. A. Oraevsky, B. Clingman, J. Zalev, A. T. Stavros, W. T. Yang, and J. R. Parikh, "Clinical optoacoustic imaging combined with ultrasound for coregistered functional and anatomical mapping of breast tumors," Photoacoustics, vol. 12, pp. 30–45, 2018, doi: 10.1016/j.pacs.2018.08.003.
24. G. L. G. Menezes et al., "Downgrading of Breast Masses Suspicious for Cancer by Using Optoacoustic Breast Imaging," Radiology, vol. 288, no. 2, pp. 355–365, 2018, doi: 10.1148/radiol.2018170500.

25. E. I. Neuschler et al., "Downgrading and Upgrading Gray-Scale Ultrasound BI-RADS Categories of Benign and Malignant Masses With Optoacoustics: A Pilot Study," Am. J. Roentgenol., vol. 211, no. 3, pp. 689–700, 2018, doi: 10.2214/AJR.17.18436.
26. E. I. Neuschler et al., "A Pivotal Study of Optoacoustic Imaging to Diagnose Benign and Malignant Breast Masses: A New Evaluation Tool for Radiologists," Radiology, vol. 287, no. 2, pp. 398–412, 2018, doi: 10.1148/radiol.2017172228.
27. T. Kitai et al., "Photoacoustic mammography: Initial clinical results," Breast Cancer Tokyo Jpn., vol. 21, Apr. 2012, doi: 10.1007/s12282-012-0363-0.
28. E. Fakhrejahani et al., "Clinical Report on the First Prototype of a Photoacoustic Tomography System with Dual Illumination for Breast Cancer Imaging," PLOS ONE, vol. 10, no. 10, pp. 1–13, Oct. 2015, doi: 10.1371/journal.pone.0139113.
29. M. Toi et al., "Visualization of tumor-related blood vessels in human breast by photoacoustic imaging system with a hemispherical detector array," Sci. Rep., vol. 7, p. 41970, Feb. 2017, doi: 10.1038/srep41970.
30. I. Yamaga et al., "Vascular branching point counts using photoacoustic imaging in the superficial layer of the breast: A potential biomarker for breast cancer," Photoacoustics, vol. 11, Jun. 2018, doi: 10.1016/j.pacs.2018.06.002.
31. Y. Matsumoto et al., "Visualising peripheral arterioles and venules through high-resolution and large-area photoacoustic imaging," Sci. Rep., vol. 8, Oct. 2018, doi: 10.1038/s41598-018-33255-8.
32. Susanne E. Vaartjes and Johan C. G. van Hespen and Joost M. Klaase and Frank M. van den Engh and Andy K. H. The and Wiendelt Steenbergen and Ton G. van Leeuwen and Srirang Manohar, "First clinical trials of the Twente Photoacoustic Mammoscope (PAM)."
33. M. Heijblom et al., "Visualizing breast cancer using the Twente photoacoustic mammoscope: What do we learn from twelve new patient measurements?," Opt Express, vol. 20, no. 11, pp. 11582–11597, May 2012, doi: 10.1364/OE.20.011582.
34. M. Heijblom et al., "Appearance of breast cysts in planar geometry photoacoustic mammography using 1064-nm excitation," J. Biomed. Opt., vol. 18, no. 12, p. 126009, 2013, doi: 10.1117/1.JBO.18.12.126009.
35. M. Heijblom et al., "Photoacoustic image patterns of breast carcinoma and comparisons with Magnetic Resonance Imaging and vascular stained histopathology," Sci. Rep., vol. 5, p. 11778, Jul. 2015, doi: 10.1038/srep11778.
36. S. Schoustra et al., "Twente Photoacoustic Mammoscope 2: system overview and three-dimensional vascular network images in healthy breasts," J. Biomed. Opt., vol. 24, p. 1, Oct. 2019, doi: 10.1117/1.JBO.24.12.121909.
37. R. Kruger, C. Kuzmiak, R. Lam, D. Reinecke, S. Rio, and D. Steed, "Dedicated 3D photoacoustic breast imaging," Med. Phys., vol. 40, p. 113301, Nov. 2013, doi: 10.1118/1.4824317.
38. L. Lin, P. Hu, J. Shi, C. M. Appleton, K. Maslov, and L. V. Wang, "Clinical photoacoustic computed tomography of the human breast in vivo within a single breath hold," in Photons Plus Ultrasound: Imaging and Sensing 2018, A. A. Oraevsky and L. V. Wang, Eds., SPIE, 2018, p. 104942X. doi: 10.1117/12.2290987.
39. L. Lin et al., "Single-breath-hold photoacoustic computed tomography of the breast," Nat. Commun., vol. 9, no. 1, p. 2352, 2018, doi: 10.1038/s41467-018-04576-z.
40. G. Diot et al., "Multispectral Optoacoustic Tomography (MSOT) of Human Breast Cancer," Clin. Cancer Res. Off. J. Am. Assoc. Cancer Res., vol. 23, no. 22, p. 6912—6922, Nov. 2017, doi: 10.1158/1078-0432.ccr-16-3200.
41. J. Kukačka et al., "Second-generation optoacoustic imaging of breast cancer patients," medRxiv, pp. 2021–10, 2021, doi: 10.1016/j.pacs.2022.100343.
42. X. L. Dean-Ben, T. Fehm, M. Gostic, and D. Razansky, "Volumetric hand-held optoacoustic angiography as a tool for real-time screening of dense breast," J. Biophotonics, vol. 9, May 2015, doi: 10.1002/jbio.201500008.
43. N. Nyayapathi et al., "Dual Scan Mammoscope (DSM)—A New Portable Photoacoustic Breast Imaging System With Scanning in Craniocaudal Plane," IEEE Trans. Biomed. Eng., vol. 67, no. 5, pp. 1321–1327, 2020, doi: 10.1109/TBME.2019.2936088.
44. S. Park, F. Brooks, U. Villa, R. Su, M. Anastasio, and A. Oraevsky, "Normalization of optical fluence distribution for three-dimensional functional optoacoustic tomography of the breast," J. Biomed. Opt., vol. 27, Mar. 2022, doi: 10.1117/1.JBO.27.3.036001.
45. W. Roll et al., "Multispectral Optoacoustic Tomography of Benign and Malignant Thyroid Disorders: A Pilot Study," J. Nucl. Med., vol. 60, p. jnumed.118.222174, Mar. 2019, doi: 10.2967/jnumed.118.222174.
46. M. Noltes et al., "Towards in vivo characterization of thyroid nodules suspicious for malignancy using multispectral optoacoustic tomography," Eur. J. Nucl. Med. Mol. Imaging, vol. 50, pp. 1–15, Apr. 2023, doi: 10.1007/s00259-023-06189-1.

47. J. Kim et al., "Multiparametric Photoacoustic Analysis of Human Thyroid Cancers In Vivo," Cancer Res., vol. 81, no. 18, pp. 4849–4860, Sep. 2021, doi: 10.1158/0008-5472.CAN-20-3334.
48. M. Yang et al., "Photoacoustic/ultrasound dual imaging of human thyroid cancers: an initial clinical study," Biomed Opt Express, vol. 8, no. 7, pp. 3449–3457, Jul. 2017, doi: 10.1364/BOE.8.003449.
49. S. Chuah et al., "Structural and functional 3D mapping of skin tumours with non-invasive multispectral optoacoustic tomography," Skin Res. Technol., vol. 23, no. 2, pp. 221–226, 2017, doi: 10.1111/srt.12326.
50. I. Stoffels et al., "Metastatic status of sentinel lymph nodes in melanoma determined noninvasively with multispectral optoacoustic imaging," Sci. Transl. Med., vol. 7, no. 317, pp. 317ra199-317ra199, 2015, doi: 10.1126/scitranslmed.aad1278.
51. B. Park et al., "3D Wide-field Multispectral Photoacoustic Imaging of Human Melanomas In Vivo: A Pilot Study," J. Eur. Acad. Dermatol. Venereol. JEADV, vol. 35, Oct. 2020, doi: 10.1111/jdv.16985.
52. D. Jüstel et al., "Spotlight on nerves: Portable multispectral optoacoustic imaging of peripheral nerve vascularization and morphology." arXiv, 2022. doi: 10.48550/ARXIV.2207.13978.
53. H. Yang et al., "Soft ultrasound priors in optoacoustic reconstruction: Improving clinical vascular imaging," Photoacoustics, vol. 19, p. 100172, 2020, doi: 10.1016/j.pacs.2020.100172.
54. A. Karlas et al., "Multispectral optoacoustic tomography of lipid and hemoglobin contrast in human carotid atherosclerosis," Photoacoustics, vol. 23, p. 100283, 2021, doi: 10.1016/j.pacs.2021.100283.
55. M. Masthoff et al., "Use of Multispectral Optoacoustic Tomography to Diagnose Vascular Malformations," JAMA Dermatol., vol. 154, Sep. 2018, doi: 10.1001/jamadermatol.2018.3269.
56. Behravesh S, Yakes W, Gupta N, Naidu S, Chong BW, Khademhosseini A, Oklu R, "Venous malformations: clinical diagnosis and treatment," Cardiovasc Diagn Ther, vol. 6, no. 6, pp. 557–569, doi: 10.21037/cdt.2016.11.10.
57. D. Razansky et al., "Multispectral Optoacoustic Tomography of Matrix Metalloproteinase Activity in Vulnerable Human Carotid Plaques," Mol. Imaging Biol. MIB Off. Publ. Acad. Mol. Imaging, vol. 14, pp. 277–85, Jul. 2011, doi: 10.1007/s11307-011-0502-6.
58. Van der Wal AC, Becker AE, "Atherosclerotic plaque rupture: pathologic basis of plaque stability and instability," Cardiovasc Res, vol. 41, no. 2, pp. 334–344, 1999, doi: 10.1016/s0008-6363(98)00276-4.
59. A. Dima and V. Ntziachristos, "In-vivo handheld optoacoustic tomography of the human thyroid," Photoacoustics, vol. 4, no. 2, pp. 65–69, 2016, doi: 10.1016/j.pacs.2016.05.003.
60. M. Kroenke et al., "Multispectral Optoacoustic Tomography: A Novel Label-Free Imaging Technique for the Assessment of hyperthyroid diseases," J. Nucl. Med., vol. 60, no. supplement 1, pp. 525–525, 2019.
61. A. Karlas et al., "Flow-mediated dilatation test using optoacoustic imaging: a proof-of-concept," Biomed Opt Express, vol. 8, no. 7, pp. 3395–3403, Jul. 2017, doi: 10.1364/BOE.8.003395.
62. Jeon BH, "Endothelial Dysfunction: From Pathophysiology to Novel Therapeutic Approaches," Biomedicines, vol. 9, no. 11, p. 1571, doi: 10.3390/biomedicines9111571.
63. I. Tsuge et al., "Photoacoustic Tomography Shows the Branching Pattern of Anterolateral Thigh Perforators In Vivo," Plast. Reconstr. Surg., vol. 141, no. 5, p. 1288—1292, May 2018, doi: 10.1097/prs.0000000000004328.
64. J. E. Lubek and S. L. Engroff, "Chapter 71 - Anterolateral Thigh Flap," in Current Therapy In Oral and Maxillofacial Surgery, S. C. Bagheri, R. B. Bell, and H. A. Khan, Eds., Saint Louis: W.B. Saunders, 2012, pp. 584–588. doi: 10.1016/B978-1-4160-2527-6.00071-2.
65. Y. Matsumoto et al., "Label-free photoacoustic imaging of human palmar vessels: A structural morphological analysis," Sci. Rep., vol. 8, Jan. 2018, doi: 10.1038/s41598-018-19161-z.
66. Y. Ishida et al., "Photoacoustic 3D imaging detects potential microvascular injuries," medRxiv, 2020, doi: 10.1101/2020.11.02.20224204.
67. S. na et al., "Massively parallel functional photoacoustic computed tomography of the human brain," Nat. Biomed. Eng., vol. 6, May 2022, doi: 10.1038/s41551-021-00735-8.
68. Alawneh JA, Hutchinson PAJ, Warburton E, "Stroke management: decompressive hemicraniectomy," BMJ Clin Evid, 2015.
69. W. Choi et al., "Three-dimensional Multistructural Quantitative Photoacoustic and US Imaging of Human Feet in Vivo," Radiology, vol. 303, no. 2, pp. 467–473, 2022, doi: 10.1148/radiol.211029.
70. J. Kim, S. Park, Y. Jung, Y. Zhang, J. Lovell, and C. Kim, "Clinical real-time photoacoustic/ultrasound imaging system at POSTECH," Mar. 2016, p. 970805. doi: 10.1117/12.2211839.
71. J. Kim et al., "Programmable Real-time Clinical Photoacoustic and Ultrasound Imaging System," Sci. Rep., vol. 6, p. 35137, Oct. 2016, doi: 10.1038/srep35137.
72. E. Merčep, X. L. Dean-Ben, and D. Razansky, "Combined Pulse-Echo Ultrasound and Multispectral Optoacoustic Tomography With a Multi-Segment Detector Array," IEEE Trans. Med. Imaging, vol. PP, pp. 1–1, May 2017, doi: 10.1109/TMI.2017.2706200.
73. A. A. Plumb, N. T. Huynh, J. Guggenheim, E. Zhang, and P. Beard, "Rapid volumetric photoacoustic tomographic imaging with a Fabry-Perot ultrasound sensor depicts peripheral arteries and microvascular

vasomotor responses to thermal stimuli," Eur. Radiol., vol. 28, pp. 1037–1045, 2018, doi: 10.1007/s00330-017-5080-9.

74. C. Lee, W. Choi, J. Kim, and C. Kim, "Three-dimensional clinical handheld photoacoustic/ultrasound scanner," Photoacoustics, vol. 18, p. 100173, 2020, doi: 10.1016/j.pacs.2020.100173.
75. C. Özsoy et al., "LightSpeed: A Compact, High-Speed Optical-Link-Based 3D Optoacoustic Imager," IEEE Trans. Med. Imaging, vol. PP, pp. 1–1, Apr. 2021, doi: 10.1109/TMI.2021.3070833.
76. Y. Skridlevskiy, I. Petrov, I. Patrikeev, R. Esenaliev, and D. Prough, "Multiwavelength optoacoustic system for noninvasive monitoring of cerebral venous oxygenation: A pilot clinical test in the internal jugular vein," Opt. Lett., vol. 31, pp. 1827–9, Jul. 2006, doi: 10.1364/OL.31.001827.
77. J. Yang, G. Zhang, S. Qiquan, M. Wu, L. Huang, and H. Jiang, "Detecting hemodynamic changes in the foot vessels of diabetic patients by photoacoustic tomography," J. Biophotonics, vol. 13, May 2020, doi: 10.1002/jbio.202000011.
78. Y. Suzuki et al., "Subcutaneous Lymphatic Vessels in the Lower Extremities: Comparison between Photoacoustic Lymphangiography and Near-Infrared Fluorescence Lymphangiography," Radiology, vol. 295, p. 191710, Feb. 2020, doi: 10.1148/radiol.2020191710.
79. Y. Suzuki, H. Kajita, N. Imanishi, S. Aiso, and K. Kishi, "Observation of a Lymphatic Pump in a Human by Using Photoacoustic Imaging," Plast. Reconstr. Surg. Glob. Open, vol. 8, p. e2914, Jun. 2020, doi: 10.1097/GOX.0000000000002914.
80. Y. Suzuki et al., "Use of photoacoustic imaging to determine the effects of aging on lower extremity lymphatic vessel function," J. Vasc. Surg. Venous Lymphat. Disord., vol. 10, May 2021, doi: 10.1016/j.jvsv.2021.05.001.
81. A. Oh et al., "Photoacoustic lymphangiography before and after lymphaticovenular anastomosis," Arch. Plast. Surg., vol. 48, pp. 323–328, May 2021, doi: 10.5999/aps.2020.02404.
82. Verhey EM, Kandi LA, Lee YS, Morris BE, Casey WJ, Rebecca AM, Marks LA, Howard MA, Teven CM, "Outcomes of Lymphovenous Anastomosis for Lower Extremity Lymphedema: A Systematic Review," Plast. Reconstr. Surg., vol. 10, no. 10, 2022, doi: 10.1097/GOX.0000000000004529.
83. Venugopal V, Pavlakis S, Duchenne Muscular Dystrophy. StatPearls, 2023. [Online]. Available: https://www.ncbi.nlm.nih.gov/books/NBK482346/
84. A. P. Regensburger et al., "Detection of collagens by multispectral optoacoustic tomography as an imaging biomarker for Duchenne muscular dystrophy," Nat. Med., pp. 1–11, 2019, doi: 10.1038/s41591-019-0669-y.
85. A. Karlas et al., "Multispectral optoacoustic tomography of muscle perfusion and oxygenation under arterial and venous occlusion: A human pilot study," J. Biophotonics, vol. 13, no. 6, p. e201960169, 2020, doi: 10.1002/jbio.201960169.
86. G. Diot, A. Dima, and V. Ntziachristos, "Multispectral opto-acoustic tomography of exercised muscle oxygenation," Opt. Lett., vol. 40, pp. 1496–9, Apr. 2015, doi: 10.1364/OL.40.001496.
87. A. P. Regensburger et al., "Multispectral optoacoustic tomography for non-invasive disease phenotyping in pediatric spinal muscular atrophy patients," Photoacoustics, vol. 25, p. 100315, 2022, doi: 10.1016/j.pacs.2021.100315.
88. H. Chaytow, K. M. E. Faller, Y.-T. Huang, and T. H. Gillingwater, "Spinal muscular atrophy: From approved therapies to future therapeutic targets for personalized medicine," Cell Rep. Med., vol. 2, no. 7, p. 100346, 2021, doi: 10.1016/j.xcrm.2021.100346.
89. J. Shubert and M. Lediju Bell, "Photoacoustic imaging of a human vertebra: Implications for guiding spinal fusion surgeries," Phys. Med. Biol., vol. 63, Jun. 2018, doi: 10.1088/1361-6560/aacdd3.
90. J. Yang et al., "Photoacoustic imaging of hemodynamic changes in forearm skeletal muscle during cuff occlusion," Biomed. Opt. Express, vol. 11, Jul. 2020, doi: 10.1364/BOE.392221.
91. McDowell C, Farooq U, Haseeb M, Inflammatory Bowel Disease. StatPearls, 2023. [Online]. Available: https://www.ncbi.nlm.nih.gov/books/NBK470312/
92. M. J. Waldner et al., "Multispectral Optoacoustic Tomography in Crohn's Disease: Noninvasive Imaging of Disease Activity," Gastroenterology, vol. 151, no. 2, pp. 238–240, 2016, doi: 10.1053/j.gastro.2016.05.047.
93. F. Knieling et al., "Multispectral Optoacoustic Tomography for Assessment of Crohn's Disease Activity," N. Engl. J. Med., vol. 376, no. 13, pp. 1292–1294, 2017, doi: 10.1056/NEJMc1612455.
94. Ha F, Khalil H, "Crohn's disease: a clinical update," Ther. Adv Gastroenterol, vol. 8, no. 6, pp. 352–9, 2015, doi: 10.1177/1756283X15592585.
95. F. Knieling et al., "Multispectral Optoacoustic Tomography in Ulcerative Colitis - A First-in-human Diagnostic Clinical Trial," J. Nucl. Med., vol. 58, no. supplement 1, pp. 1196–1196, 2017.
96. M. Gajendran et al., "A comprehensive review and update on ulcerative colitis," Dis. Mon., vol. 65, no. 12, p. 100851, 2019, doi: 10.1016/j.disamonth.2019.02.004.
97. F. Knieling et al., "Contrast-enhanced Multispectral Optoacoustic Tomography for Functional Assessment of the Gastrointestinal Tract," Dec. 2022, doi: 10.21203/rs.3.rs-2380754/v1.

98. L.-P. Paulus et al., "Multispectral optoacoustic tomography of the human intestine – temporal precision and the influence of postprandial gastrointestinal blood flow," Photoacoustics, vol. 30, p. 100457, 2023, doi: 10.1016/j.pacs.2023.100457.
99. C.-P. Adler, "Inflammatory Joint Diseases," in Bone Diseases: Macroscopic, Histological, and Radiological Diagnosis of Structural Changes in the Skeleton, Berlin, Heidelberg: Springer Berlin Heidelberg, 2000, pp. 441–455. doi: 10.1007/978-3-662-04088-1_13.
100. P. J. van den Berg, K. Daoudi, H. J. B. Moens, and W. Steenbergen, "Feasibility of photoacoustic/ultrasound imaging of synovitis in finger joints using a point-of-care system," Photoacoustics, vol. 8, pp. 8–14, 2017, doi: 10.1016/j.pacs.2017.08.002.
101. O. Abeyakoon et al., "Optoacoustic imaging detects hormone-related physiological changes of breast parenchyma," Ultraschall Med.-Eur. J. Ultrasound, vol. 40, no. 06, pp. 757–763, 2019, doi: 10.1055/a-0628-6248.
102. Thiyagarajan DK, Basit H, Jeanmonod R, Physiology, Menstrual Cycle. StatPearls, 2023. [Online]. Available: https://www.ncbi.nlm.nih.gov/books/NBK500020/
103. L. Monteiro Rodrigues, T. F. Granja, and S. F. de Andrade, "Optoacoustic Imaging Offers New Insights into In Vivo Human Skin Vascular Physiology," Life, vol. 12, no. 10, 2022, doi: 10.3390/life12101628.
104. Rosenberry R, Nelson MD, "Reactive hyperemia: a review of methods, mechanisms, and considerations," Am J Physiol Regul Integr Comp Physiol, vol. 318, no. 3, pp. 605–618, 2020, doi: 10.1152/ajpregu.00339.2019.
105. I. Tsuge et al., "Preoperative vascular mapping for anterolateral thigh flap surgeries: A clinical trial of photoacoustic tomography imaging," Microsurgery, vol. 40, Nov. 2019, doi: 10.1002/micr.30531.
106. H. Shimizu et al., "Three-dimensional visualization of thoracodorsal artery perforators using photoacoustic imaging," J. Plast. Reconstr. Aesthet. Surg., vol. 75, no. 9, pp. 3166–3173, 2022, doi: 10.1016/j.bjps.2022.06.016.
107. A. A. Amin, M. Rifaat, A. Farahat, and T. Hashem, "The role of thoracodorsal artery perforator flap in oncoplastic breast surgery," J. Egypt. Natl. Cancer Inst., vol. 29, no. 2, pp. 83–87, 2017, doi: 10.1016/j.jnci.2017.01.004.
108. K. Nagae et al., "Real-time 3D Photoacoustic Visualization System with a Wide Field of View for Imaging Human Limbs," F1000Research, vol. 7, p. 1813, Feb. 2019, doi: 10.12688/f1000research.16743.2.
109. N.-A. Fasoula et al., "Multicompartmental non-invasive sensing of postprandial lipemia in humans with multispectral optoacoustic tomography," Mol. Metab., vol. 47, p. 101184, 2021, doi: 10.1016/j.molmet.2021.101184.
110. L. Grünherz et al., "Preoperative Mapping of Lymphatic Vessels by Multispectral Optoacoustic Tomography," Lymphat. Res. Biol., vol. 20, no. 6, pp. 659–664, 2022, doi: 10.1089/lrb.2021.0067.
111. J. Aguirre et al., "Precision assessment of label-free psoriasis biomarkers with ultra-broadband optoacoustic mesoscopy," Nat. Biomed. Eng., vol. 1, p. 0068, 10/online 2017, doi: 10.1038/s41551-017-0068 https://www.nature.com/articles/s41551-017-0068#supplementary-information.
112. W. Bost, R. Lemor, and M. Fournelle, "Optoacoustic Imaging of Subcutaneous Microvasculature With a Class one Laser," IEEE Trans. Med. Imaging, vol. 33, May 2014, doi: 10.1109/TMI.2014.2326552.
113. J. Yang, G. Zhang, M. Wu, S. Qiquan, L. Huang, and H. Jiang, "Photoacoustic assessment of hemodynamic changes in foot vessels," J. Biophotonics, vol. 12, p. e201900004, Mar. 2019, doi: 10.1002/jbio.201900004.
114. E. Z. Zhang et al., "Multimodal photoacoustic and optical coherence tomography scanner using an all optical detection scheme for 3D morphological skin imaging," Biomed Opt Express, vol. 2, no. 8, pp. 2202–2215, Aug. 2011, doi: 10.1364/BOE.2.002202.
115. B. Zabihian et al., "In vivo dual-modality photoacoustic and optical coherence tomography imaging of human dermatological pathologies.," Biomed. Opt. Express, vol. 6 9, pp. 3163–78, 2015, doi: 10.1364/BOE.6.003163.
116. J. Aguirre, M. Schwarz, D. Soliman, A. Buehler, M. Omar, and V. Ntziachristos, "Broadband mesoscopic optoacoustic tomography reveals skin layers," Opt Lett, vol. 39, no. 21, pp. 6297–6300, Nov. 2014, doi: 10.1364/OL.39.006297.
117. J. Aguirre et al., "Assessing nailfold microvascular structure with ultra-wideband raster-scan optoacoustic mesoscopy," Photoacoustics, vol. 10, pp. 31–37, 2018, doi: 10.1016/j.pacs.2018.02.002.
118. H. He et al., "Fast Optoacoustic Mesoscopy of Microvascular Endothelial Dysfunction in Cardiovascular Risk and Disease," bioRxiv, 2021, doi: 10.1101/2021.09.28.462150.
119. H. He et al., "Optoacoustic skin mesoscopy opens a window to systemic effects of diabetes," Jun. 2020, doi: 10.1101/2020.06.29.20142273.
120. M. Schwarz, A. Buehler, J. Aguirre, and V. Ntziachristos, "Three-dimensional multispectral optoacoustic mesoscopy reveals melanin and blood oxygenation in human skin in vivo," J. Biophotonics, vol. 9, Nov. 2015, doi: 10.1002/jbio.201500247.

 doi:10.20944/preprints202404.1202.v2

121. M. Schwarz, J. Aguirre, D. Soliman, A. Buehler, and V. Ntziachristos, "Unmixing chromophores in human skin with a 3D multispectral optoacoustic mesoscopy system," in Photons Plus Ultrasound: Imaging and Sensing 2016, A. A. Oraevsky and L. V. Wang, Eds., in Society of Photo-Optical Instrumentation Engineers (SPIE) Conference Series, vol. 9708. Mar. 2016, p. 970855. doi: 10.1117/12.2209333.
122. B. Hindelang et al., "Optoacoustic mesoscopy shows potential to increase accuracy of allergy patch testing," Contact Dermatitis, vol. 83, no. 3, pp. 206–214, 2020, doi: 10.1111/cod.13563.
123. B. Hindelang et al., "Quantification of skin sensitivity to ultraviolet radiation using ultra-wideband optoacoustic mesoscopy," Br. J. Dermatol., vol. 184, Aug. 2020, doi: 10.1111/bjd.19463.
124. O. Braun-Falco, G. Plewig, H. H. Wolff, and R. K. Winkelmann, "Erythematous and Erythematosquamous Skin Diseases," in Dermatology, Berlin, Heidelberg: Springer Berlin Heidelberg, 1991, pp. 403–466. doi: 10.1007/978-3-662-00181-3_14.
125. A. Berezhnoi, M. Schwarz, A. Buehler, S. V. Ovsepian, J. Aguirre, and V. Ntziachristos, "Assessing hyperthermia-induced vasodilation in human skin in vivo using optoacoustic mesoscopy," J. Biophotonics, vol. 11, no. 11, p. e201700359, 2018, doi: 10.1002/jbio.201700359.
126. S. Moustakidis, M. Omar, J. Aguirre, P. Mohajerani, and V. Ntziachristos, "Fully Automated Identification of Skin Morphology in Raster-Scan Optoacoustic Mesoscopy using Artificial Intelligence," Med. Phys., vol. 46, Jul. 2019, doi: 10.1002/mp.13725.
127. J. Aguirre et al., "Precision assessment of label-free psoriasis biomarkers with ultra-broadband optoacoustic mesoscopy," Nat. Biomed. Eng., vol. 1, p. 0068, May 2017, doi: 10.1038/s41551-017-0068.
128. B. Hindelang et al., "Enabling precision monitoring of psoriasis treatment by optoacoustic mesoscopy," Sci. Transl. Med., vol. 14, no. 644, p. eabm8059, 2022, doi: 10.1126/scitranslmed.abm8059.
129. S. J. Ford et al., "Structural and functional analysis of intact hair follicles and pilosebaceous units by volumetric multispectral optoacoustic tomography," J. Invest. Dermatol., vol. 136, no. 4, pp. 753–761, 2016, doi: https://doi.org/10.1016/j.jid.2015.09.001.
130. Y. Yew et al., "Raster-scanning optoacoustic mesoscopy (RSOM) imaging as an objective disease severity tool in atopic dermatitis patients," J. Am. Acad. Dermatol., vol. 84, Jun. 2020, doi: 10.1016/j.jaad.2020.06.045.
131. Maser, Raelene E and Nielsen, Viggo K and Bass, Eric B and Manjoo, Qurashia and Dorman, Janice S and Kelsey, Sheryl F and Becker, Dorothy J and Orchard, Trevor J, "Measuring Diabetic Neuropathy: Assessment and Comparison of Clinical Examination and Quantitative Sensory Testing," Diabetes Care, vol. 12, no. 4, pp. 270–275, 1989, doi: 10.2337/diacare.12.4.270.
132. Feldman, Eva L and Stevens, M J and Thomas, P K and Brown, M B and Canal, N and Greene, D A, "A Practical Two-Step Quantitative Clinical and Electrophysiological Assessment for the Diagnosis and Staging of Diabetic Neuropathy," Diabetes Care, vol. 17, no. 11, pp. 1281–1289, 1994, doi: 10.2337/diacare.17.11.1281.
133. G. A. Van Norman, "Drugs, Devices, and the FDA: Part 2: An Overview of Approval Processes: FDA Approval of Medical Devices," JACC Basic Transl. Sci., vol. 1, no. 4, pp. 277–287, Jun. 2016, doi: 10.1016/j.jacbts.2016.03.009.
134. A. V. Kaplan et al., "Medical device development: from prototype to regulatory approval," Circulation, vol. 109, no. 25, pp. 3068–3072, Jun. 2004, doi: 10.1161/01.CIR.0000134695.65733.64.